AD________________

GRANT NUMBER DAMD17-96-1-6143

TITLE: Exploration of Monoenergetic X-Ray Mammography with Syncrotron Radiation

PRINCIPAL INVESTIGATOR: Richard E. Johnston, Ph.D.

CONTRACTING ORGANIZATION: University of North Carolina
at Chapel Hill
Chapel Hill, North Carolina 27599-1350

REPORT DATE: July 1997

TYPE OF REPORT: Annual

PREPARED FOR: Commander
U.S. Army Medical Research and Materiel Command
Fort Detrick, Maryland 21702-5012

REPORT DOCUMENTATION PAGE

Form Approved
OMB No. 0704-0188

1. AGENCY USE ONLY *(Leave blank)*

2. REPORT DATE
July 1997

3. REPORT TYPE AND DATES COVERED
Annual (1 Jul 96 - 30 Jun 97)

4. TITLE AND SUBTITLE
Exploration of Monoenergetic X-Ray Mammography with Syncrotron Radiation

5. FUNDING NUMBERS
DAMD17-96-1-6143

6. AUTHOR(S)
Johnston, Richard E., Ph.D.

7. PERFORMING ORGANIZATION NAME(S) AND ADDRESS(ES)
University of North Carolina at Chapel Hill
Chapel Hill, North Carolina 27599-1350

8. PERFORMING ORGANIZATION REPORT NUMBER

9. SPONSORING / MONITORING AGENCY NAME(S) AND ADDRESS(ES)
U.S. Army Medical Research and Materiel Command
504 Scott Street
Fort Detrick, Maryland 21702-5012

10. SPONSORING / MONITORING AGENCY REPORT NUMBER

11. SUPPLEMENTARY NOTES

12a. DISTRIBUTION / AVAILABILITY STATEMENT
Approved for public release; distribution unlimited

12b. DISTRIBUTION CODE

13. ABSTRACT *(Maximum 200 words)*

The purpose of this research is to explore the potential advantages of monoenergetic x-rays in medical imaging especially mammography.
We are using synchrotron radiation as our source of x-rays to provide monoenergetic beams from 16 keV upward. We are also developing Monte Carlo techniques to calculate contrast images.
To date we have demonstrated an increase in contrast in phantoms and tissue samples over that obtained with conventional x-ray machines. We are developing a Monte Carlo based 2D image model with better documentation of the scatter that can display the image from which image-contrast can be calculated. We have also initiated exploration of refraction imaging and diffraction enhancement imaging that can be obtained by "analyzing" the emerging beam from target phantoms. This imaging technique promises to offer a new concept in medical imaging that could improve contrast more than an order of magnitude.

14. SUBJECT TERMS
Breast Cancer
Synchrotron, monoenergetic x-rays, mammography

15. NUMBER OF PAGES
47

16. PRICE CODE

17. SECURITY CLASSIFICATION OF REPORT	18. SECURITY CLASSIFICATION OF THIS PAGE	19. SECURITY CLASSIFICATION OF ABSTRACT	20. LIMITATION OF ABSTRACT
Unclassified	Unclassified	Unclassified	Unlimited

NSN 7540-01-280-5500

Standard Form 298 (Rev. 2-89)
Prescribed by ANSI Std. Z39-18 298-102

USAPPC V1.00

FOREWORD

Opinions, interpretations, conclusions and recommendations are those of the author and are not necessarily endorsed by the U.S. Army.

___ Where copyrighted material is quoted, permission has been obtained to use such material.

___ Where material from documents designated for limited distribution is quoted, permission has been obtained to use the material.

RES Citations of commercial organizations and trade names in this report do not constitute an official Department of Army endorsement or approval of the products or services of these organizations.

___ In conducting research using animals, the investigator(s) adhered to the "Guide for the Care and Use of Laboratory Animals," prepared by the Committee on Care and Use of Laboratory Animals of the Institute of Laboratory Resources, National Research Council (NIH Publication No. 86-23, Revised 1985).

RES For the protection of human subjects, the investigator(s) adhered to policies of applicable Federal Law 45 CFR 46.

___ In conducting research utilizing recombinant DNA technology, the investigator(s) adhered to current guidelines promulgated by the National Institutes of Health.

___ In the conduct of research utilizing recombinant DNA, the investigator(s) adhered to the NIH Guidelines for Research Involving Recombinant DNA Molecules.

___ In the conduct of research involving hazardous organisms, the investigator(s) adhered to the CDC-NIH Guide for Biosafety in Microbiological and Biomedical Laboratories.

R. Eugene Mentos 7/28/97

PI - Signature Date

1. TABLE OF CONTENTS

2. Introduction:

The x-ray emission from a synchrotron provides the capability of obtaining high photon fluxes, selectable monoenergetic x-ray beams and a nearly ideal narrow beam geometry that is maintained, i.e. non divergent, over great distances from the source. Thus, the synchrotron provides the ideal x-ray imaging source particularly for imaging of soft tissues such as the breast. Scatter radiation which is present in the x-ray beam after it passes through the object being imaged, degrades the image quality and reduces the contrast between the various tissues and structures within the breast. The use of an analyzer placed in the beam emerging from the imaged object, provides a beam with no scatter component to the image detector. Thus, the synchrotron x-ray imaging system should provide us with the maximum detectability possible with a transmission x-ray system.

We are exploring the use of the monoenergetic x-rays using both phantom objects and real tissue samples. We are experimentally comparing the synchrotron images to images obtained from conventional polyenergetic x-ray imaging systems. We are developing a Monte Carlo simulation program to determine the energy to achieve optimum contrast and compare to the polyenergetic x-ray images.

We also are investigating the feasibility of using an analyzer crystal in the x-ray beam after being transmitted through the sample inorder to reject any scattering that occurs in the sample.

Background (exerpted from original proposal)

A small number of experimenters have explored the use of monoenergetic x-rays for medical imaging other than mammography [1,2,3]. Carroll, et.al.[4] have shown that there are significant differences in attenuation between normal and cancerous tissues for monoenergetic x-rays in the range of 14 to 18 keV. Boone and Seibert [5] did a computer simulation to compare performance of monoenergetic x-rays to polyenergetic x-rays from tungsten anode systems with regard to imaging. Their conclusion was that monoenergetic sources exhibited a 40 to 200 % improvement in tissue contrast when imaging the chest with different contrast targets. Admittedly, soft tissue contrast benefited the least. Burattini, et.al, [6,7] recently published their work using synchrotron radiation to image both breast phantoms and specimens. They conclude that the images obtained with monoenergetic x-rays have higher contrast, better resolution and similar, or less, radiation dose compared to the conventional polyenergetic x-ray images.

The following is a summary of our experience using a monoenergetic x-ray beam from the National Synchrotron Light Source (NSLS) at Brookhaven National Laboratory to explore the potential of monoenergetic photons for mammographic imaging.

Our preliminary experiments [8] showed that we could obtain image contrast somewhat superior to that from conventional x-ray images, but due to instrumentation problems we had very noisy images. With improved instrumentation (scanning motor drive system, new monochromotor and clean beryllium windows on the beam port) we have been able to reduce the noise considerably. We have imaged various mammographic phantoms including the ACR, an anthropomorphic phantom, and a Contrast Detail phantom. We have also imaged a breast tissue sample. All of our experiments were carried out at energies from 16 keV to 24 keV.

3. BODY

The following is a description of the experimental methods used for our studies. The beam of x-rays emerging from the bending magnet on the NSLS synchrotron is polyenergetic ranging from a few keV to above 50 keV. To obtain monoenergetic x-rays, a double crystal Si(111) Laue monochromator is placed in the beam. This monochromator produces a beam with a bandwidth of about 5 to 10 eV in the energy range used here (16 - 24 keV). The energy is set by the angle the crystal makes with the incident synchrotron beam (the Bragg angle). The vertical position of the beam is essentially fixed over the small energy range used in these experiments, thus shielding and component alignment do not have to change when the energy is changed. Changing energies is accomplished by driving the angle of the monochromator to the Bragg angle and adjusting the second crystal to give a maximum response.

A beam collimator is placed at the exit of the monochromator to shield against stray radiation, another slit is located approximately 110 cm in front of the object to be imaged, and a final slit between the object and the imaging plate serves as an anti-scatter slit. Because of the high beam intensity, an aluminum absorber is placed in the monochromator beam to reduce the intensity to a level that can be handled by the detector after the beam has passed through the phantom. It is necessary to attenuate the beam by a factor of more than 100. This was accomplished by use of the absorber and by working with a vertical beam size of 0.5 mm. The overall length of the system from monochromator to detector plate is 2.8 meters. To form an image, the imaging plate and the object are scanned through the beam. The total scan field is 85 x 85 mm. This is large enough to image phantoms and tissue samples. The drive system is a stepping motor translation stage with a speed that is varied under computer control to limit the radiation dose to the detector to a predetermined level.

The Laue crystal "analyzer" is a thin Si(111) crystal placed in the beam between the object being imaged and the imaging detector. A portion of the beam is diffracted and imaged on the image receptor. The significance of the Laue diffracted image is that it is essentially free of scatter from the sample. That is because the scattered x-rays are at lower energy and travel in directions different from the primary monochromator beam. The scattered rays are not diffracted by the Laue crystal which is set at the Bragg angle for the primary beam energy and direction. The Laue crystal analyzer is thus an ideal scatter rejection optic. Since the Laue analyzer also transmits a fraction of the incident beam, a non diffracted image is obtained simultaneously on the imaging receptor.

Two NSLS design ion chambers placed in the beamline are used to determine the dose to the sample (or entrance dose). Although they perform close to the theoretical limit in their response, initial experiments were done to verify the response using TLD dosimeters. The first ion chamber (in front of the imaging shutter) measures the strength of the monochromatic beam. The experiment control computer calculates the proper rate of vertical translation of the sample for a predetermined exposure to the image detector based on the measured monochromatic beam intensity. The second ion chamber is behind the slits and directly in front of the sample. Since it accepts all of the beam which actually strikes the sample, it is used, along with the known translation rate, to calculate the actual exposure dose to the sample.

The image detector used to obtain digital image data is a Fuji HR-V photostimulable storage phosphor plate (PSP). This is a high resolution plate used with an AC3 Fuji reader (Fuji Medical Systems Stamford, Ct.). A sensitivity of 400 was used to read the plates since this is the lowest sensitivity available on the reader. The plates are read out at a 2560 x 2048 matrix (100 mm /pixel) resolution. For the film images, we used mammographic film

(Fuji UM MA-HC) and a mammographic screen (Fuji UM Fine). The films are processed using a tabletop film processor (Film Quick-CT; Imaging Marketing Corp. Mesa, AZ). Film speed and contrast are monitored sensitometrically. The conventional mammography system is a Siemens Mammomat 2 (Siemens Medical Systems, Iselin, NJ). Fuji mammography film (Fuji UM MA-HC), and screen (Fuji UM Fine) is used and a bucky grid with a 4:1 grid ratio and 27 lines/cm. Processor chemistry used is Picker 3-7-90 type S developer and Picker Spectre fixer.

For quantitative measurements of contrast, A Gammex RMI model 180 Contrast Detail phantom (Gammex RMI, Middleton, WI.) is used which has target Lucite disks varying from 1mm to 0.06 mm thickness and diameters varying from 7 mm down to 0.3 mm machined into a Lucite substrate. The phantom is 15 mm thick and to obtain greater thickness, Lucite slabs are added to the phantom. For subjective assessment, the American College of Radiology (ACR) phantom , and a Gammex RMI model 165 anthropomorphic phantom are used.

During the first year of this grant, we have made two experimental runs at NSLS. June, '96, and Nov. '96, and a third experimental run from May 28 to June 8, '97 at the Advanced Photon Source, Argonne Natl. Laboratory. We obtained two mastectomy specimens in one of which we implanted a mouse tumor (1 cm3 volume), and the second we implanted four 1 cm diam.plastic disks ranging from 0.5mm to 2.0 mm thickness. We x-rayed these samples, along with the ACR, Anthropomorphic, and CD phantoms with the conventional polyenergetic x-ray machine using film and then imaged them with monoenergetic x-rays at 16, 18, and 20 keV using both film and a Fuji plate as the detector. In all cases the synchrotron images at 16 keV showed improved contrast over the conventional images. The implanted mouse tumor was not detectable in any of the images. During the June '96 run, we also explored the use of the "analyzer" crystal in the emerging beam. The expectation was that we should improve the contrast to some extent by removing small angle scatter that would pass through the collimator slits. It also offered us the opportunity to simultaneously explore the concept of refraction imaging. That is, as the x-rays pass through the tissue sample, various tissues have different indices of refraction and the "analyzer", a Bragg reflection crystal, provides the means for generating an image of these refractive indices differences, a property independent of energy and a different type of tissue property[10]. We imaged the ACR phantom and the tissue sample with implanted plastic disks. The resulting images were of two types, 1) an x-ray absorption image, 2) a refractive index image. In both cases, we were able to visualize details of the ACR phantom not seen before, and the refractive image of the tissue sample more clearly outlined the disks than either the conventional x-ray or the 16 keV monoenergetic x-ray image. Thus, we demonstrated the feasibility of refractive index imaging and generated an x-ray absorption with contrast an order of magnitude beyond that expected. See appendix 3.

Between June '96 and Nov. '96, we investigated the physics behind the increased contrast obtained in the absorption image and theorized that structural content of the object in the beam can cause low angle diffraction (milliradians) that is screened out by the "analyzer" crystal. At the Nov. run, we proposed testing a "Laue analyzer" which is a transmission crystal that would allow both directly transmitted x-rays and refracted x-rays to be recorded simultaneously on the same Fuji plate detector. The advantage would be to avoid image registration problems. Unfortunately, we had various instrumentation problems, our detector / sample transport system generated noise and the Laue analyzer alignment was unsuccessful. As a result, we had to revert to the Bragg analyzer to generate images. We had two biological samples for this run, a laboratory mouse and a fetal pig. Both objects had been imaged with a conventional x-ray machine. However, due to the experimental problems, the images were not useful.

The last run, May 28 to June 8 at the Synchrotron Radiation Instrumentation Collaborative Access Team (SRICAT) 1-BM-B bending magnet beam line at the Advanced Photon Source at Argonne National Laboratory, was intended to explore higher imaging energies. However instrumentation problems compromised the experiment at higher energies. We did discover a method that almost entirely removes vibrations and have now obtained the best Diffraction Enhanced Images (DEI) to date. We were able to verify and obtain data which supports our contention that a major source of contrast in the DEI technique is due to the scatter rejection property (extinction contrast). Coupled with refraction contrast, the DEI system can produce image contrast based on the objects absorption, refraction and extinction characteristics.

Images of a formalin preserved mouse (BioC) with an implanted benign dog skin tumor is shown in figures 1 - 3. Figure 1 is a "normal" radiograph taken without the analyzer in place as a reference image to compare the DEI images with. Figure 2 shows the apparent absorption and refraction image of the same mouse. These images are derived from images taken at +/- 1.5 microradians on each side of the analyzer rocking curve. It is clear from the refraction image that the tumor has been implanted in the leg of the mouse. The refraction image shows the crater formed when the tumor was pushed into the tissue which was not visible in the absorption image or normal radiograph and clearly show that the refraction image can identify edges of features in the object. It also show that we must develop better models for testing our technique. Figure 3 is a composite image showing the normal radiograph, an image taken at the peak of the analyzer rocking curve the DEI images, shown in figure 2, and images taken further off the peak of the analyzer curve at +/1 3 microradians. In all cases it is clear that new information is obtained by the DEI technique.

Figures 4 - 6 shows a subcutaneous mass from a dog's leg placed in beef tissue preserved in formalin (BioA). The normal radiograph is shown in figure 4. The mass is roughly a circular object on the left side of the image. The DEI apparent absorption and refraction images are shown in figure 5. Again the refraction image highlights the edges surrounding the implanted tumor. The DEI apparent absorption image appears similar to the normal radiograph, however, in performing images at larger rocking curve angles, it appears that the dog tumor may have a lack of small angle scattering and lack of complex refraction compared to the surrounding beef tissue. This is shown in figure 6, the summary image of BioA at the bottom in the +/- 3 microradian images. this is our first indication that the DEI technique may be sensitive to a extinction or refraction contrast in cancerous tissue.

The consequence of these two new sources of contrast is very relevant to mammography and medical imaging in general. These contrast sources are energy independent effects as opposed to absorption. Conventional radiography depends on the object absorbing x-rays to create the radiograph of the internal structure of the object. Refraction and scattering as imaged by our system does not change as the imaging energy is raised. Absorption contrast is lost, but the refraction and scattering (extinction) contrast remain. This raises the possibility of successfully applying this technique at high x-ray energy if refraction or extinction contrast can be demonstrated in cancerous tissue surrounded by normal tissues. This will be the focus of future work.

Finally, during the first year, we have developed a Monte Carlo simulation code that can produce 2D images. This code uses the point-detector scheme to produce an image without the quantum mottle normally associated with Monte Carlo images. The code handles simple geometries to simulate the experimental setup at the NSLS. An example of an image generated by the code is in Figure 7. Calculated contrasts from each of the structures in the phantom are listed in Table 1.

Using the Monte Carlo code, scattered photons can be counted separately from unscattered photons, showing how the scatter degrades the contrast (Figure 8). We have found the angular distribution of scatter is quite different from the theoretical models that most Monte Carlo simulations use. In order to determine the scattered contribution accurately in our calculations, we are measuring the actual scattering distribution from different biological tissues including fat, muscle and water. Some preliminary measurements have been made using a powder diffraction x-ray machine and more accurate measurements will be made at NSLS.

The code is still being developed to include accurate modeling of the digital detector and polyenergetic source. The code will also use advanced Monte Carlo techniques to determine sensitivities of doses and contrast to various input parameters, such as tissue density or cross section.

4. CONCLUSIONS:

The first year of this grant has enabled us to explore the use of monoenergetic x-rays for possible improvement in detecting low contrast abnormalities in breast tissue. We have demonstrated that the use of monoenergetic x-rays can improve the contrast in phantom studies and we have made progress in developing a Monte Carlo code that can be used to generate a 2D image and can be used for modeling the effect of changing various parameters of the x-ray system on the image. We have also demonstrated the feasibility of generating an x-ray absorption image with increased contrast due to diffraction enhancement and a totally new type of tissue characterization image based on refractive index gradients within the tissue.

5. REFERENCES:

1. Thomlinson W. Medical Applications of Synchrotron Radiation. Nucl. Instr. and Meth. 1992; A319 , 295-304.
2. Luccio A. Synchrotron Radiation and Biomedical imaging. Phys Med 1988; vol IV,N.1 (suppl.1): 87-117.
3. Mori H, Hyodo K, Tobita K, et. al. Visualization of Penetrating Transmural Arteries In Situ by Monoenergetic Synchrotron Radiation. Circulation, 1994; 89:863-871.
4. Carrol F, Waters J, Andrews W, et. al. Attenuation of Monochromatic X-Rays by Normal and Abnormal Breast Tissues. Investigative Radiology 1994; 29, 266-272.
5. Boone JM, and Seibert JA. A Comparison of mono- and poly-energetic x-ray beam performance for radiographic and fluorscopic imaging. Med. Phys. 1994; 21 (12), 1853-1863.
6 Burattini E, Gambaccini M, Indovina PL, et. al. Synchrotron radiation: A new source in x-ray mammography. Radiol. Med. 1992; 4, pp181-188.
7. Burattini E, Cossu E, Di Maggio C, et. al. X-ray Mammography with Synchrotron Radiation: A New High resolution Technique Valid for Clinical Application. Radiology 1994; 195, 239-244.
8. Johnston RE, Washburn D, Pisano P, et. al. Preliminary experience with monoenergetic photon mammography. Medical Imaging 1995: Physics of Medical Imaging, SPIE 1995; vol. 2432, 434-441.
9. Chapman D, Thomlinson W, Arefeli F, Gmur N, Zhong Z, Menk R, Johnston E, Washburn D, Pisano E, Sayers D. "Mammography Imaging Studies Using a Laue Analyzer Crystal". Rev.Sci. Instrum. 1996: 67(9), CD-ROM.

Publications :

1. Johnston RE, Washburn D, Pisano E, Burns C, Thomlinson WC, Chapman D, Arfelli F, Gmur NF, Zhong Z, Sayers D. Mammography Phantom Studies with Synchrotron Radiation. Radiology 1996: 200, 659-663.
2. Chapman D, Thomlinson W, Arefeli F, Gmur N, Zhong Z, Menk R, Johnston E, Washburn D, Pisano E, Sayers D. "Mammography Imaging Studies Using a Laue Analyzer Crystal". Rev.Sci. Instrum. 1996: 67(9), CD-ROM.
3. Chapman D, Thomlinson W, Johnston RE, Washburn D, Pisano E, Gmur N, Zhong Z, Menk R, Arfelli F, Sayers D. Diffraction Enhanced X-Ray Imaging. accepted for publication in Physics in Medicine and Biology, 1997.

6. APPENDICES:

APPENDIX 1

DEI Images

APS Experiment Results
BioC Images - Normal

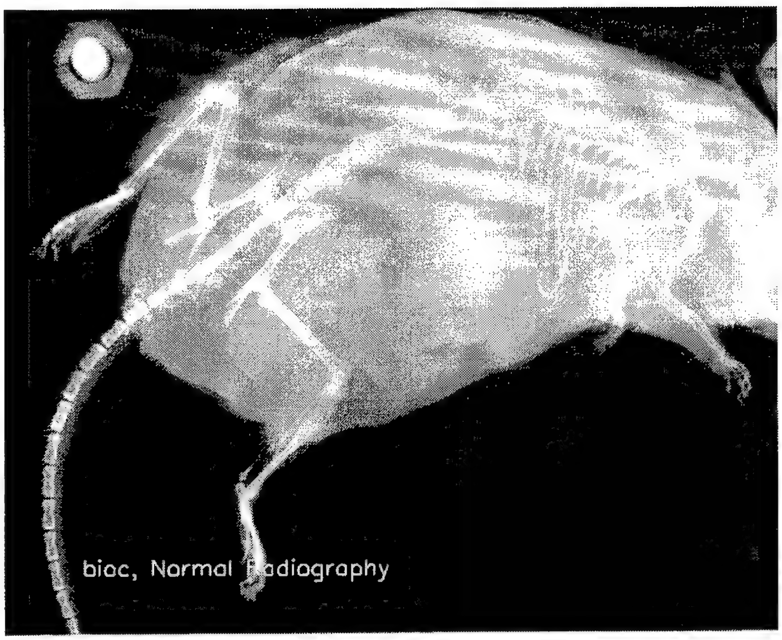

Normal Radiograph

7/24/97

Figure 1

APS Experiment Results
BioC Images - DEI

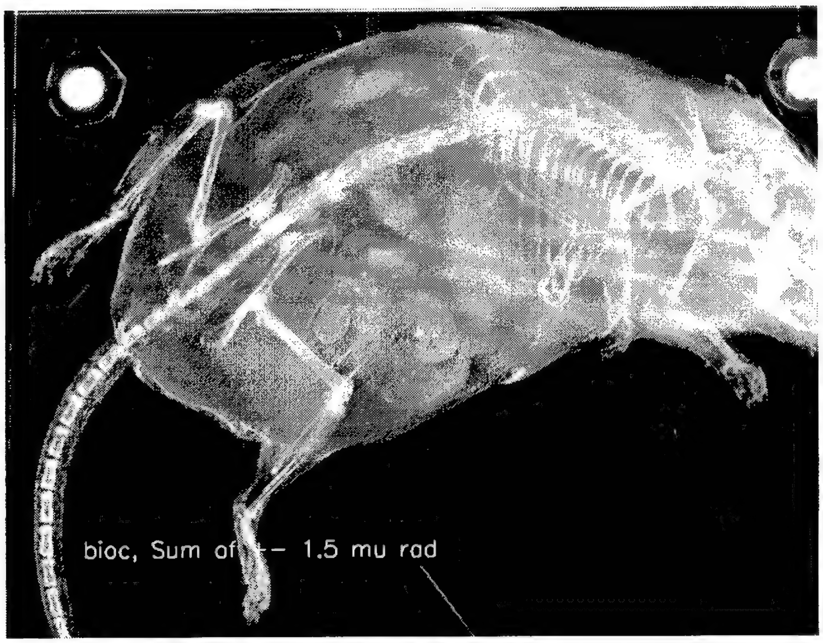

Apparent Absorption Image (sum)

Refraction Image (difference)

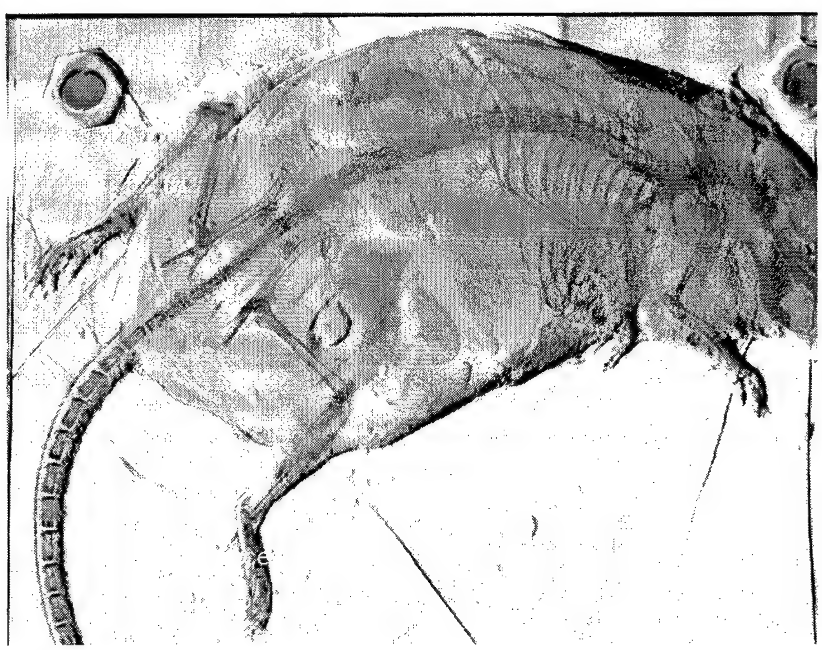

7/24/97

Figure 2

APS Experiment Results
BioC Summary

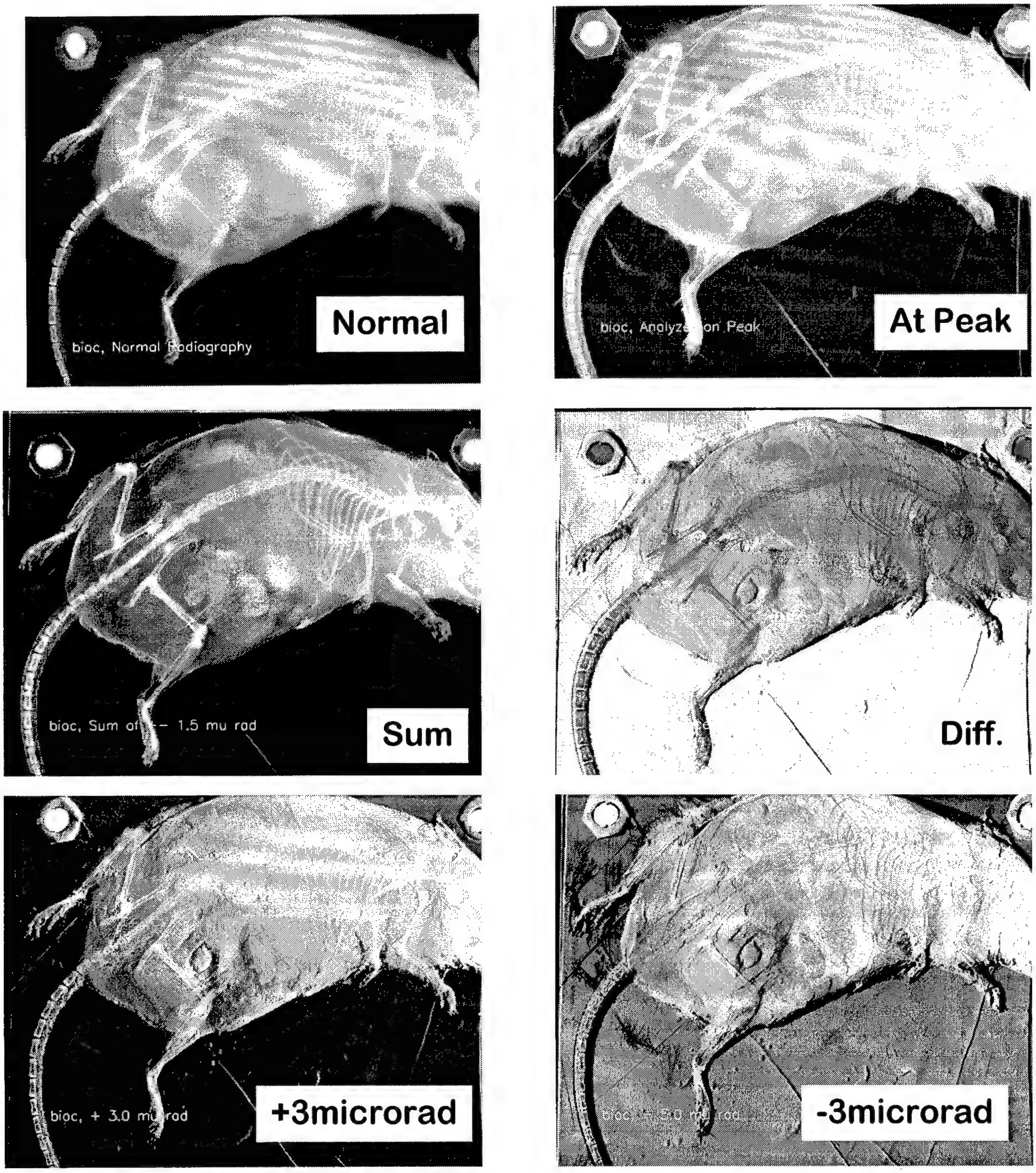

7/24/97

Figure 3

APS Experiment Results
BioA Images - Normal

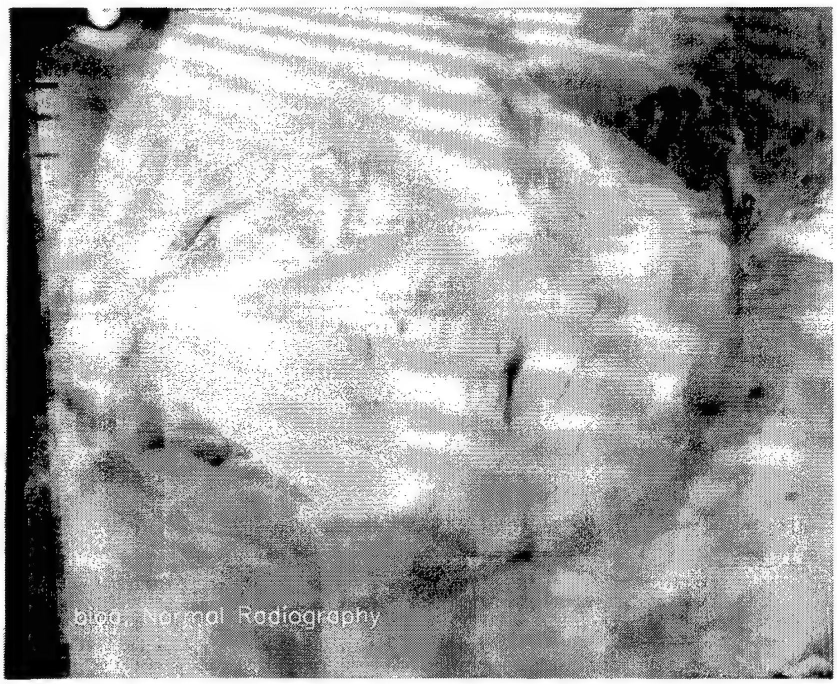

Normal
Radiograph

Figure 4

7/24/97

APS Experiment Results
BioA Images - DEI

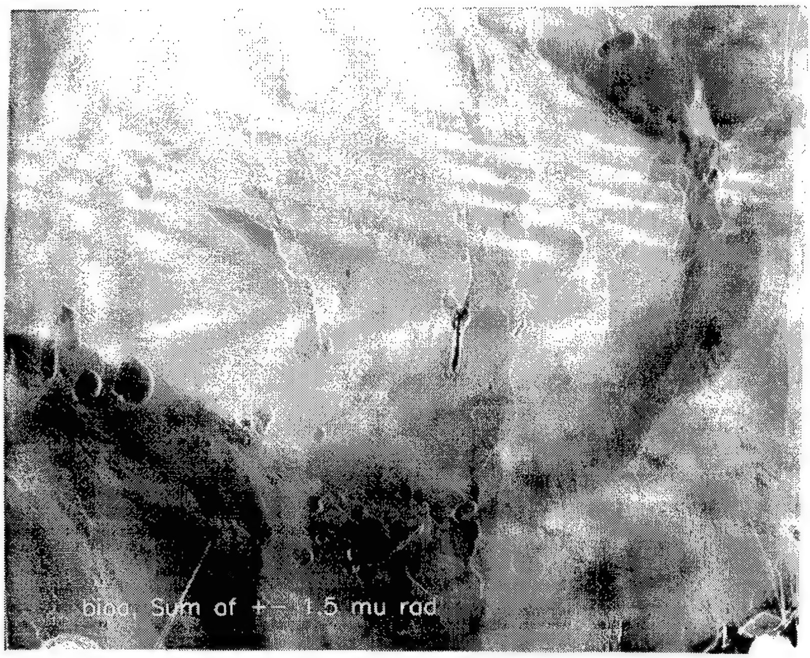

Apparent Absorption Image (sum)

Refraction Image (difference)

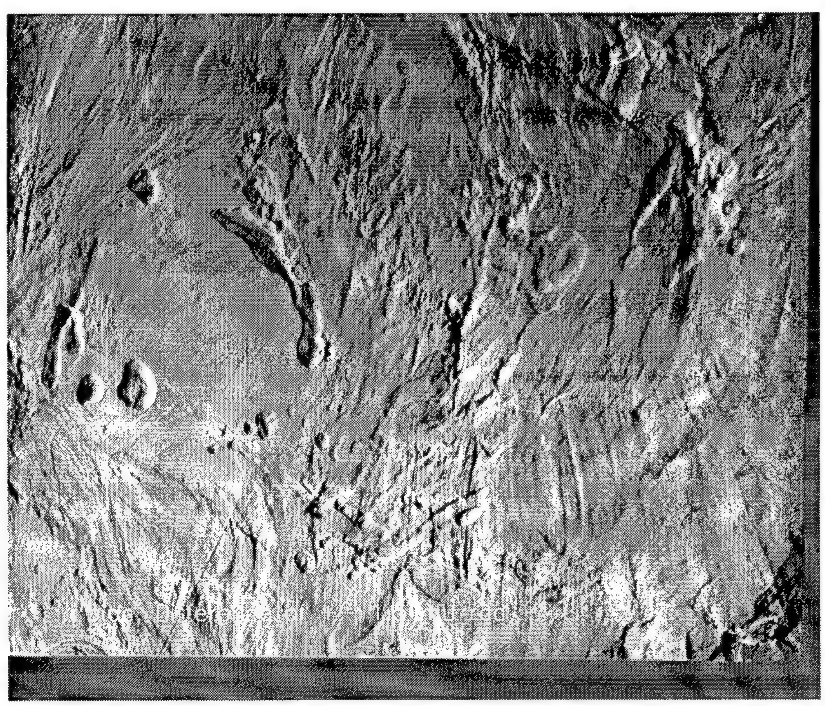

7/24/97

Figure 5

APS Experiment Results
BioA Summary

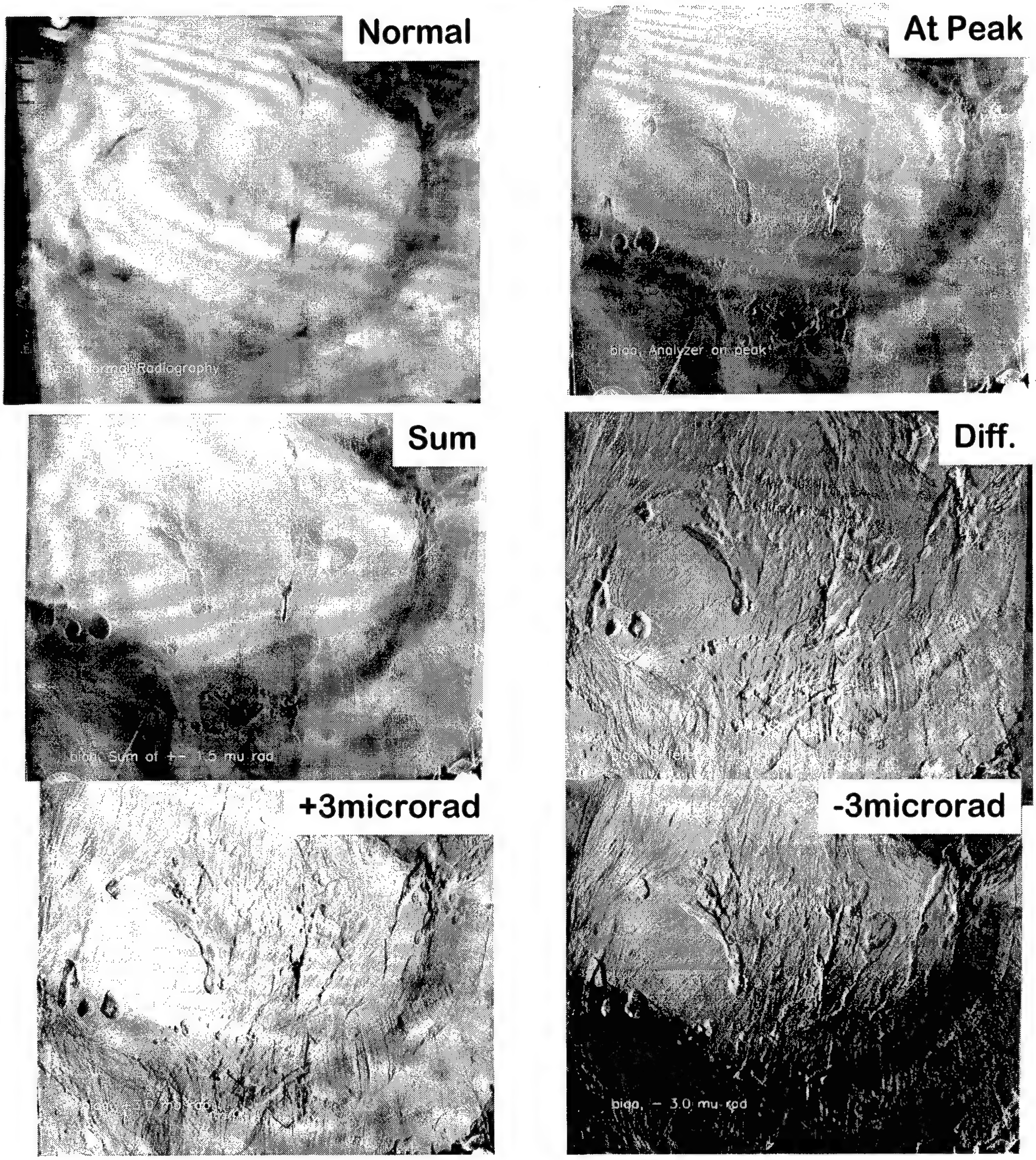

7/24/97

Figure 6

APPENDIX 2

Monte Carlo Simulation

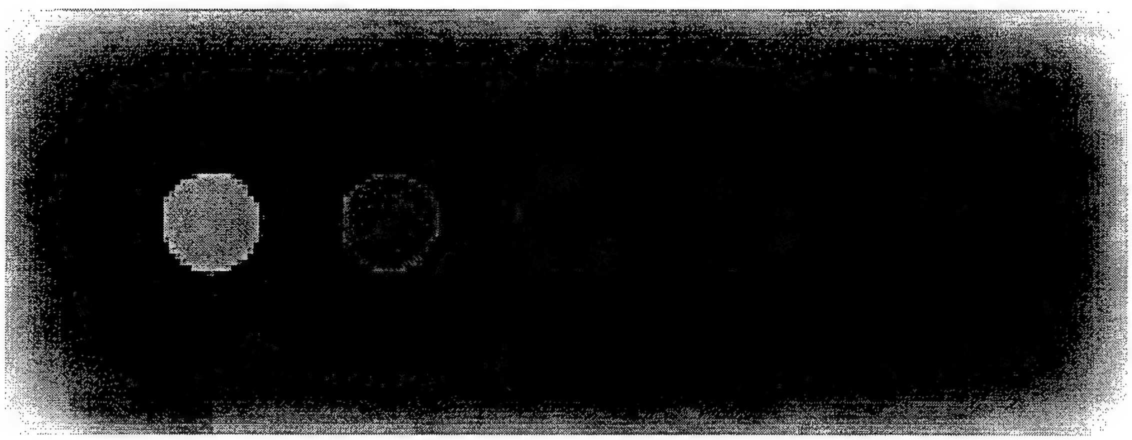

Figure 7: Image from an 18 keV polarized beam striking a portion of the contrast detail phantom. This portion is 8 cm by 3 cm with structures of 0.707 cm diameter and thickness of 0.1 cm (left side) to 0.025 cm, simulating a density change of 6.67% to 1.67%. The pixel size is 400 μm by 400 μm.

Table 1: Calculated contrast from the unscattered and total image.

Thickness (cm)	Unscattered Contrast	With Scatter Contrast
0.1000	0.085	0.062
0.0707	0.060	0.043
0.0500	0.042	0.029
0.0354	0.030	0.024
0.0250	0.021	0.016

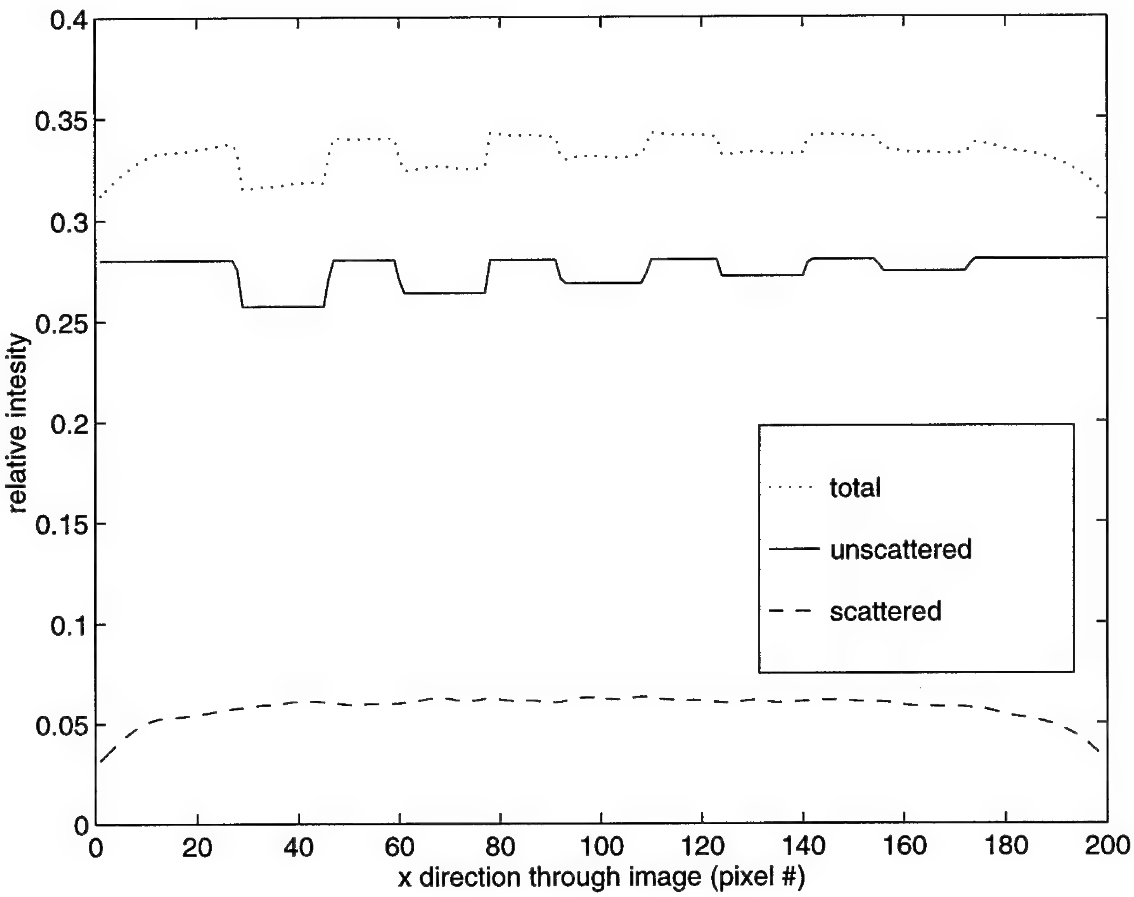

Figure 8 Centerline from simulation image. The scattered photons add intensity to the image plate everywhere, decreasing contrast.

APPENDIX 3

Manuscript accepted for publication in Physics in Medicine and Biology

Diffraction Enhanced X-ray Imaging

D. Chapman(1), W. Thomlinson(2), R. E. Johnson(3), D. Washburn(3), E. Pisano(3), N. Gmür(2), Z. Zhong(2), R. Menk(4), F. Arfelli(5), D. Sayers(6)

(1) CSRRI, Illinois Institute of Technology, 3101 S. Dearborn, Chicago, IL 60616 USA

(2) National Synchrotron Light Source, Brookhaven National Laboratory, Upton, NY 11973, USA

(3) University of North Carolina, Chapel Hill, NC 27599 USA

(4) Universität GHS Siegen, 57068 Siegen, Germany

(5) Societa' Sincrotrone Trieste e Sezione dell' INFN - Trieste, Italy

(6) North Carolina State University, Raleigh, NC 27695 USA

Abstract

Diffraction enhanced imaging is a new x-ray radiographic imaging modality using monochromatic x-rays from a synchrotron which produces images of thick absorbing objects that are almost completely free of scatter. They show dramatically improved contrast over standard imaging applied to the same phantom. The contrast is based not only on attenuation but also the refraction and diffraction properties of the sample. This imaging method may improve image quality for medical applications, industrial radiography for non-destructive testing, and x-ray computed tomography.

1. Introduction

Diffraction Enhanced Imaging (DEI), is a new x-ray radiographic imaging modality which is a product of a research program designed to explore a monoenergetic line scan system for radiography of thick absorbing objects (Johnston *et al* 1996). The x-ray source is from the X27C beamline at the National Synchrotron Light Source. Synchrotron radiation provides x-rays which are intense, vertically collimated, polarized, and continuous over a wide energy range (Margaritondo, 1988). These highly desirable qualities allows a wide variety of imaging research to be done at a synchrotron (Thomlinson 1992, 1994).

For this study a crystal monochromator is used to select a small energy band from the incident synchrotron radiation which forms the imaging beam which strikes the object. One aspect of this program has been the use of an additional crystal like the type used in the monochromator as a scatter rejection optic that diffracts the beam which is transmitted through the object being imaged. This additional crystal is called an analyzer crystal or just analyzer. Experiments performed with the analyzer revealed that this system was sensitive to refractive index effects within the object in addition to the x-ray absorption and scattering by the object. The early experiments indicated that from two images acquired using an analyzer crystal, a simple algorithm could be used to separate refractive index effects from the absorption effects (Chapman *et al* 1996). These pilot experiments were performed using a transmission case (Laue geometry) analyzer to simultaneously obtain a transmission image and a diffracted image.

Definitive experiments and analysis have now been performed to explore the use of a reflection case (Bragg geometry) analyzer crystal arrangement to decompose two diffracted images into an independent refraction image and an apparent absorption image. Apparent absorption means the combined absorption and extinction processes. Extinction is the loss of intensity due to diffraction occurring as the beam traverses the object. The type of extinction referred to is commonly called secondary extinction (Zachariasen 1963). Images taken with the new system are presented which show contrast at least an order of magnitude greater than the measured values for synchrotron x-ray images of the same object acquired using the conventional transmission imaging modality. These images are of thick objects containing at least a 36mm acrylic plastic thickness. In fact, images from this new modality show additional information that is not available with standard radiography.

An algorithm is presented here for the case of a Bragg analyzer which can be used to decompose the images into separate refraction and apparent absorption components. The same algorithm can be applied to the diffracted images in the Laue case. The diffracted images are essentially scatter free, since the crystal prevents much of the scatter from reaching the detector. The refraction image is shown to have high sensitivity for delineating the boundaries of those regions in the object which have different refractive indices. An explanation of the sources of the enhanced image contrast is also given which shows that the increased contrast is a result of extinction effects. This opens new opportunities for imaging based on these properties. Since the contrast of an image based on extinction can be much higher than contrast based on x-

ray attenuation, detection of smaller inhomogeneities, like tumors in medical images or microfractures in industrial parts, should be feasible.

The ability of the monochromator and analyzer system to resolve refraction effects does not depend on the imaging energy. However, the scattering properties of various elements are energy dependent, which may allow optimization of the imaging system energy to maximize contrast due to extinction while maintaining refraction contrast. Thus, the new modality may be optimally applied at higher x-ray energies, which would allow for better penetration in non-destructive testing or lower doses in medical imaging.

Other researchers have applied diffractive optics to imaging problems (Beliaevsky *et al* 1991, Somenkov *et al* 1996, Podurets *et al* 1989) and have observed refraction effects. However, the method described here quantifies and produces images of the refraction and absorption independently for the first time. Recently, there has been interest in phase contrast imaging which makes use of the high transverse coherence of third generation synchrotron sources. Phase contrast images are limited to either thin objects or high x-ray imaging energies (Davis *et al* 1995, Nugent *et al* 1996, Wilkins *et al* 1996). The DEI technique in the present work does not depend on phase contrast and works with thick samples.

2. Physical Principles of DEI

A radiograph using monoenergetic x-rays contains several components; a coherently scattered component, an incoherently scattered component, and the

transmitted beam. Part of the transmitted beam may be refracted in the sample through a very small angle (microradians) due to refractive index gradients in the object. In the x-ray range refractive index gradients arise from variations in ρt along the beam path, where ρ is the density and t is the thickness. A fraction of the transmitted beam may also be diffracted by organized structures within the sample through angles of the order of milliradians (small angle scattering). I_C, I_I, and I_D are the portions of the coherent scattering, incoherent scattering, and diffraction intensity which arrive on the detector along with I_R. I_R is the portion of the incident beam which has only been affected by refraction and attenuated by absorption and extinction. The recorded intensity, I_N, in a radiograph can be expressed as

$$I_N = I_R + I_D + I_C + I_I \qquad \text{Equation 1}$$

Variations in I_N across the field of view of the detector are the sources of contrast in normal radiography (formally $\Delta I_N/I_N$). The DEI modality will separate I_R from the other components and will show contrast based on refraction, absorption and extinction.

The scattering components, I_C and I_I, contribute to loss of contrast and spatial resolution. Some improvement can be obtained by using synchrotron radiation and a monochromator to select the energy (Johnston *et al* 1996, Burattini *et al* 1994). However it has been shown that considerable additional gain in contrast can be realized by adding crystal diffraction optics between the object and the imaging system. This refinement almost completely removes the scatter contribution to the image since only

x-rays aligned within the angular acceptance of a crystal analyzer will be diffracted onto the detector. I_C and I_I are eliminated as contributions to the image. The angular acceptance is called the rocking curve of the crystal (Zachariasen 1945). For the x-ray energies and crystal reflections used here, the width of this curve is a few microradians.

Since the diffraction angles in the sample being imaged are typically a few milliradians (small angle scattering), most of I_D is rejected by the crystal. It is this rejection of small angle scattering in particular which gives rise to the sensitivity to the loss of direct beam intensity which has been "small angle scattered". In diffraction research, the term used for the loss of direct beam intensity due to scattering is called secondary extinction (Zachariasen 1945, 1963). Normally, the small angle scattered x-rays will not be distinguished from the direct beam and will appear in a radiograph of the object. Thus in normal radiography there will be no extinction contrast.

The rejection of the scattered x-rays leaves only I_R, the intensity of x-rays transmitted through the sample with a direction very close to the initial direction of the beam. This beam may have been refracted slightly as it passes through the sample (of the order of microradians).

In DEI two images are acquired, one on each side of the rocking curve of the Bragg analyzer. Each image contains information about the object's apparent absorption and refraction. Since the analyzer crystal orientation is chosen to diffract the beam in the vertical plane, it is sensitive only to the vertical component, $\Delta\theta_Z$, of the refracted x-rays.

The intensity diffracted by the analyzer set at a relative angle θ from the Bragg angle θ_B where $\theta_B + \theta$ is the angle between the incident beam and diffraction planes is given by

$$I_B = I_R R(\theta_B + \theta) \quad \text{Equation 2}$$

where $R(\theta)$ is the analyzer reflectivity.

For DEI the analyzer is set to $\theta = \pm\Delta\theta_D/2$ where $\Delta\theta_D$ is the full width at half maximum of the rocking curve (Darwin width). This is the point of steepest slope of the rocking curve. For an incident x-ray which is not deviated in passing through the sample and incident upon the analyzer at this angle the reflectivity will be 0.5. If the x-ray emerging from the object is refracted by $\Delta\theta_Z$ then the diffracted intensity will be

$$I_B = I_R R(\theta_B \pm \frac{\Delta\theta_D}{2} + \Delta\theta_Z) \quad \text{Equation 3.}$$

For refracted x-rays there will be a variation in intensity due to the slope of the rocking curve. For example, with $\Delta\theta_D/2$ positive (high angle side) a beam refracted with $\Delta\theta_Z > 0$ is diffracted by the analyzer with reflectivity less than 0.5. A beam refracted with $\Delta\theta_Z < 0$ is diffracted by the analyzer with reflectivity greater than 0.5. If the alignment of the analyzer crystal was such that $\Delta\theta_D/2$ was negative (low angle side) this effect would be reversed since the derivative of the rocking curve, $dR/d\theta$, is of opposite sign. The steeper the slope, the greater the intensity variation due to refraction effects in the two images. For a deviation of more than $\Delta\theta_D/2$ the reflectivity will not be unique and refraction effects cannot be resolved. This is shown in figure 1a which

shows the locations on the rocking curve where the images are taken. Also shown in figure 1 are images taken on the high and low angle sides of the rocking curve which will be discussed later. In the regions of the phantom which were imaged, the refraction angles were within ± 0.2 microradians, placing all possible angles within a limited region of the rocking curve (about 5 microradians).

At $\pm\Delta\theta_D/2$ where the slope of the rocking curve is fairly constant and for small values of $\Delta\theta_Z$, $R(\theta_0+\Delta\theta_Z)$ can be expressed as a two-term Taylor series approximation

$$R(\theta_0 + \Delta\theta_Z) = R(\theta_0) + \frac{dR}{d\theta}(\theta_0)\Delta\theta_Z \qquad \text{Equation 4}$$

The intensity of the images taken on the low angle side (θ_L) and the high angle side (θ_H) of the rocking curve are,

$$I_L = I_R[R(\theta_L) + \frac{dR}{d\theta}(\theta_L)\Delta\theta_Z] \qquad \text{Equation 5a}$$

$$I_H = I_R[R(\theta_H) + \frac{dR}{d\theta}(\theta_H)\Delta\theta_Z] \qquad \text{Equation 5b}$$

These two equations can be solved for the intensity affected by apparent absorption, I_R, and for the refraction angle image, $\Delta\theta_Z$, the angle through which I_R is refracted in the z direction in traversing the object. The solutions are

$$I_R = \frac{I_L \frac{dR}{d\theta}(\theta_H) - I_H \frac{dR}{d\theta}(\theta_L)}{R(\theta_L)\frac{dR}{d\theta}(\theta_H) - R(\theta_H)\frac{dR}{d\theta}(\theta_L)} \qquad \text{Equation 6a}$$

$$\Delta\theta_Z = \frac{I_H R(\theta_L) - I_L R(\theta_H)}{I_L \frac{dR}{d\theta}(\theta_H) - I_H \frac{dR}{d\theta}(\theta_L)} \qquad \text{Equation 6b}$$

This algorithm is applied on a pixel-by-pixel basis to the diffracted images from the high and low angle side of the rocking curve.

3. Methods

The experiments were performed at the X27C beamline at the National Synchrotron Light Source (NSLS) at Brookhaven National Laboratory. The experimental setup is shown in Figure 2. The white synchrotron beam was made nearly monochromatic by a silicon double crystal monochromator which is located approximately 22m from the source of radiation. The tunable energy range of this system was 16 keV-25 keV. For the measurements described here the beam energy was 18 keV with an energy width of about 1.5 eV. The monochromator crystals used the silicon (3,3,3) lattice planes. This choice of lattice planes increased the sensitivity to refraction effects by a factor of five from the previous experiments that used the (1,1,1) lattice planes because of the narrower rocking curve of the (3,3,3) reflection (Chapman *et al* 1996). The imaging beam was approximately 80 mm wide and 0.1 mm high at the location of the object. The beam passed through a gas ionization chamber, used for monitoring the intensity of the direct beam, and a set of Lucite absorbers that reduced the beam intensity. A rotary shutter was used to control the exposure and limit unnecessary scatter at the detector position. A second ion chamber was used to measure the radiation exposure at the surface of the object. Images taken with and without the analyzer were at exposure levels comparable to conventional mammography x-ray systems. The object to be imaged was mounted on a scanning stage that was driven by a stepping motor. The x-ray beam transmitted through the object could be either imaged directly as in normal radiography or following diffraction in the vertical plane by the silicon Bragg analyzer. Radiation exposure to the image plate was controlled by

adjusting the scan speed to maintain an exposure of about 1.3μC/kg (5mR) to the plate. Typical scanning times for these experiments were on the order of 4 to 200 seconds. These limits were dictated by our scanning motors and mechanical system.

The synchrotron images were obtained by maintaining a constant exposure (~1.3μC/kg) to the image plate. In acquiring the DEI images the phantom was exposed to four times the exposure compared to the non-analyzer synchrotron radiographs. A factor of two in increased exposure compensates for the 0.5 reflectivity of the Bragg analyzer crystal and another factor of two increased exposure compensates for the two images on each side of the rocking curve.

The detector was a photo-stimulative phosphor image plate, typically used for radiology (Fuji Medical Systems high resolution HR5 and standard resolution ST5 image plates). The image recorded on the plate was digitized, stored and displayed by a Fuji Medical Systems AC3 reader and workstation. The image plates were read out at 2560 x 2048 matrix size which results in an image of 100 microns per pixel (0.1 x 0.1 mm^2).

The diffraction angle of the analyzer crystal could be finely tuned using a stepper-motor driven translation stage pushing on a long bar attached to an axle to which the crystal was attached (tangent arm). The resolution limit of the tangent arm was one microradian which was sufficient for placing the Bragg analyzer crystal at a selected position on its rocking curve.

Because the initial interest was in studying the use of synchrotron imaging for early detection of breast cancers, a mammography phantom was used as the test object to be radiographed. The standard phantom used for quality control in mammography is the American College of Radiology (ACR) phantom manufactured by Gammex RMI: Model 156. It contains features which simulate lesions commonly found in breast tissue, namely tumor-like masses (lens-shaped objects of different thickness' and diameters), simulated micro-calcifications arranged as vertices of five-point stars and cylindrical nylon fibrils (Johnston et al 1996, Arfelli et al 1996). The features are fixed in a wax block contained in a thick acrylic base. This phantom approximates a 40 to 45 mm thick compressed breast. Since the x-ray beam is a fan in the horizontal plane (x-y plane), the object and the image plate were simultaneously translated in the vertical direction (z-direction). This scanning was accomplished by a computer controlled stepper motor translation stage which held both the phantom support and a mount for the image plate cassette.

4. Results

Images taken of the ACR phantom for a conventional x-ray tube source and a monoenergetic synchrotron beam without the analyzer are shown in figures 3a and 3b, respectively. The synchrotron radiographs typically showed an increase in contrast compared with images from the conventional system (Johnston et al 1996). The conventional radiographs were taken with a Siemens Mammomat 2 using Fuji mammography film (UM MA-HC), Fuji screen (UM Fine), and grid (4:1 ratio 27 lines/cm). The ACR image was obtained at 25kVp, phototimed, 60mAs. The

synchrotron radiograph, figure 3b, was obtained with the synchrotron setup described in the Methods section above, except that the analyzer crystal was removed to allow a radiograph to be taken of the ACR phantom and the vertical beam size was increased to 0.5 mm. The image was taken at 18keV x-ray energy, with 43 μC/kg exposure to the phantom. The scanning speed was 5.33 mm/sec with an exposure time of 16.7 seconds. A Fuji ST5 image plate was used to record the image.

The low and high angle Bragg analyzer images are shown in figures 1b and 1c, respectively. Each of these images were taken with an increased exposure to the phantom of 84 μC/kg to maintain the same exposure to the image plate due to the 1/2 reflectivity of the analyzer crystal. These images were acquired at a scan speed of 0.54 mm/s with an exposure time of 165 seconds. The exposures were made onto a Fuji HR5 image plate.

Careful inspection of the images in figure 1 show that the edges of features in the images are enhanced and highlighted as if a shadow is cast on a three-dimensional surface. This shadowing effect is reversed between the images. This is most visible from the two fibrils at the top right corners of the images. This effect is due to the images being taken on opposite slopes of the rocking curve. Coherent, incoherent and small-angle scattering outside of the rocking curve (I_D diffraction) are not present in these images, leaving only the beam affected by apparent absorption and refraction (I_R from equation 1). Any rays which deviate by even a few microradians from the incident direction and/or which deviate in energy by more than a few electron volts from the energy of the incident beam will not be diffracted by the analyzer. It is clear that the

images in figure 1 taken with the analyzer have vastly superior contrast compared with the images in figures 3a and b.

Figures 4a and b show the apparent absorption image, I_R, and the refraction angle image $\Delta\theta_Z$, calculated from the decomposition algorithm (equations 6a and b) applied to the images shown in figures 1b and c. Since these images are derived from the two Bragg images, they are also scatter free.

The refraction image is, in effect, an image of the gradient of the refractive index of the object and hence capable of delineating very clearly the boundaries of regions in the object where the refractive index changes sharply. In effect, this produces an image edge-enhancement in the Bragg images. Contrast in the refraction image arises from refractive index gradients along the beam path. This explains the three-dimensional shadowed look of the image. A good example of the refraction is to inspect the fibril simulation in the upper right hand corner of Figure 4a. This object is a right circular cylinder and acts like a cylindrical lens. Thus the upper half will refract the x-rays in the opposite sense from the lower half. The refraction image is very useful in highlighting boundaries or edges in heterogeneous regions within the object. One may thus expect the refraction image to be highly useful in non-destructive examination of microcracks or other types of minute flaws.

The I_R image is a map of the intensity remaining after all the loss mechanisms have been taken out. Virtually all scatter is missing except for a small portion which falls within the angular acceptance of the analyzer. The image is dominated by the

apparent absorption which is normal absorption plus extinction. The ACR phantom is a good example of a material whose absorption and scatter are such that the sum in a normal transmission image (figure 3a) significantly degrades the contrast of the objects. For example, consider the simulated tumor mass in the upper left hand corner of figure 3b and figure 4b. The measured contrast of this 2.0 mm thick mass is summarized in table 1. The exposures used to obtain the images and the intensities measured from the images are shown. The intensities shown result from raw image plate data and are linearized since the raw data appear in logarithmic form. The I column values arise from the average background intensity in the vicinity of the embedded object. ΔI is the average change in intensity from the background in the middle of the object. Contrast is the ratio of these two values. The noise level, δI, is the standard deviation of the intensity, I (from the same region over which I has been averaged). The contrast measured from the synchrotron radiograph taken without an analyzer in figure 3b gives a measured contrast of 1.5% $\Delta I_N/I_N$. However, the same mass in figure 1b taken on the low angle side of the rocking curve gives a measured contrast of 41% $\Delta I_R/I_R$. The contrast of the apparent absorption image shown in figure 4b calculated using equation 6a has a contrast of 40%. **The diffracted beam images from the analyzer alone have produced a contrast which is about 27 times greater than that in a synchrotron radiograph taken without an analyzer!** The apparent absorption image has similar contrast, but has a lower noise level since it results from a combination of two images.

The contrast has also been measured for the 0.54mm diameter microcalcification simulation (largest of the star pattern dots above and to the right of the largest tumor

simulation at the bottom of figures 1, 3, and 4). This microcalcification has a measured contrast of 9.5% in the synchrotron radiograph shown in figure 3b. The image taken with the analyzer, figure 1b, has a measured contrast of 33%.

This startling contrast cannot be explained by normal absorption but is due to intensity loss caused by extinction. The mass created a significant amount of small angle scatter which was removed from the Bragg diffracted images. This loss of intensity will appear as an apparent absorption within the object and hence as highly enhanced contrast in the image. It is suggested that this contrast enhancement effect be called extinction contrast.

The images in figure 4 demonstrate the usefulness of DEI for imaging objects based on their refraction properties and their ability to diffract (based on the spatial order or structure within the object). This raises the possibility of distinguishing between objects of the same elemental composition, but whose scattering properties are different based on structural order.

5. Conclusion

We believe that this new imaging technique may provide significant improvements in mammography and other areas of radiology, medical or non-medical. The unique ability of this system to provide an essentially scatter free image of the object's apparent absorption as well as an image of the refraction effects may provide radiologists with sufficient additional information to allow detection of malignancies at an earlier stage than presently possible, even in patients with dense breasts. Since the

ability of the monochromator and analyzer system to resolve refraction effects and reject scattering does not depend on the imaging energy, there is a possibility that DEI may be optimally applied at higher x-ray energies, thus allowing dose reduction and in the case of mammography, less breast compression.

More studies using real tissues and anthropomorhic phantoms must be done to come to the conclusion that this technique can lead to a better method of breast imaging,. There is the possibility that the enhanced contrast may detract from the ability detect cancerous tissue due the complexity of the structures involved. These issues will be the topic of future research.

Acknowledgments

The authors would like to thank Fuji Medical Systems for the loan of the AC3 image plate reader system and technical support in setting up and operating the unit. Also, we would like to thank Dr. D. Peter Siddons for the use of the X27C beamline and Ms. B. Dowd for assistance in setting up and operating the beamline. We thank Dr. I. Ivanov for preparing the analyzer crystals used in these experiments. This work was supported in part by a US Army grant DAMD17-96-1-6143 and at the National Synchrotron Light Source by US Department of Energy Contract DE-AC02-76CH00016 and ARPA contract AOB227.

References

Arfelli F, Burns C, Chapman D, Gmür N, Johnston R E, Menk R, Pisano E, Sayers D, Thomlinson W, Washburn D and Zhong Z 1995 *Brookhaven National Laboratory Informal Report, BNL-62935*

Beliaevsky E A, Epfanov V P, and Ingal V N 1991 *Soviet Patent No. 4934958* and 1992 *US Patent No. 5319694.*

Burattini E, Cossu E, DiMaggio C, Gambaccini M, Indovina P, Marziani M, Porek M, Simeoni S and Simonetti G 1994 *Radiology* **195**, 239-44

Chapman D, Thomlinson W, Arfelli F, Gmür N, Zhong Z, Menk R, Johnston R E, Washburn D, Pisano E and Sayers D 1996 *Rev. Sci. Instrum.*, **67**(9), published on CD-ROM

Davis T J, Gao D, Gureyev T E, Stevenson A W and Wilkins 1995 S W, *Nature* **373**, 595-8

Davis T J, Gureyev T E, Gao D, Stevenson A W and Wilkins S W 1995 *Phys. Rev. Lett.* **74**, 3173-5

Johnston R E, Washburn D, Pisano E, Burns C, Thomlinson W C, Chapman L D, Arfelli F, Gmür N, Zhong Z and Sayers D 1996 *Radiology* **200**, 659-63

Margaritondo 1988 *Introduction to Synchrotron Radiation* (New York: Oxford University Press)

Nugent K A, Gureyev T E, Cookson D F, Paganin D and Barnea Z 1996 *Phys. Rev. Lett.*, **77**, 2961-4

Podurets K M, Somenkov V A, Shil'shtein S Sh 1989 *Sov. Phys. Tech. Phys.* **34**, 654-7

Somenkov V A, Tkalich A K and Shil'shtein S Sh 1991 *Sov. Phys. Tech. Phys.* (Brief Communication) **36**, 1309-11

Thomlinson W 1992 *Nucl. Instr. Meth.*, **A319**, 295-304

Thomlinson W 1994 *Medical Applications of Synchrotron Radiation at the National Synchrotron Light Source* from *Synchrotron Radiation in the Biosciences* (ed. B. Chance, et. al.) 674-680 (Oxford University Press, New York)

Wilkins S W, Gureyev T E, Gao D, Pogany A and Stevenson A W 1996 *Nature* **384** 335-8

Zachariasen W H 1945 *Theory of X-Ray Diffraction in Crystals* (New York: John Wiley and Sons) Chapter 4

Zachariasen W H 1963 Acta Cryst **16** 1139-1144

Correspondence and requests for materials should be directed to: Prof. Dean Chapman, CSRRI, 3101 South Dearborn, Illinois Institute of Technology, Chicago, Illinois 60616, e-mail: chapman@sparky.csrri.iit.edu

Figure Captions

Figure 1. (a) The Si (3,3,3) analyzer rocking curve at 18 keV (solid line-calculated, stars-measured points). The calculation includes the effects of the beam diffracted by the double crystal monochromator. An image is taken on each side of the peak, shown by the vertical lines. Any refraction near these vertical lines is varied in intensity due to the slope of the rocking curve, as shown in the inset. The range of refraction angles occurring in the ACR phantom is ±0.2 microradians, creating intensity variations of ±5%. (b) The intensity recorded on the image plate using the low angle side of the rocking curve. (c) The high angle side image. Notice that the contrast of the fibrils has switched between the two images.

Figure 2. A schematic diagram of the Bragg geometry setup in the X27C experimental hutch at the NSLS. The image in figure 1b was made using a similar setup, only without the Bragg crystal analyzer in place. Not shown in the diagram are the sets of collimators just before the sample and just before the image plate, which help to reduce air scatter and scatter from the sample reaching the detector.

Figure 3. Images of the ACR phantom. (a) A conventional image taken with a Siemens Mammomat II (Siemens Medical Systems, Iselin, NJ) mammography x-ray machine operated at 25 kVp. (b) An image taken using monoenergetic synchrotron radiation at 18 keV without an analyzer crystal in place.

Figure 4. The decomposed images obtained from the images in figures 1b and c using equations 6a and b. (a) The refraction angle image. (b) The apparent absorption image.

Tables

Table 1. Conventional and DEI Contrast Determination for a Tumor Simulation and a Microcalcification from the American College of Radiology Quality Assurance Phantom.

			Signal*			Noise*	
Image	Exposure to Phantom	Embedded Object	I	ΔI	ΔI/I	δI	δI/I
Synchrotron Radiograph (figure 3b)	43μC/kg	Tumor Simulation	16.6	0.25	0.015	±0.10	±0.006
		Micro-calcification	16.3	1.55	0.095	±0.09	±0.006
Synchrotron DEI (low angle image, figure 1c)	84μC/kg	Tumor Simulation	9.5	3.9	0.41	±0.28	±0.030
		Micro-calcification	11.5	3.72	0.33	±0.17	±0.015
Apparent Absorption Image (combined image, figure 4b)	168μC/kg	Tumor Simulation	18.8	7.6	0.40	±0.25	±0.013
		Micro-calcification	21.3	5.13	0.24	±0.26	±0.012

* Values are taken from image plate data with no background subtraction. Data has been linearized using $I_{LINEAR} = e^{\frac{N_{RAW}}{255.0}}$ where N_{RAW} is the raw data value.

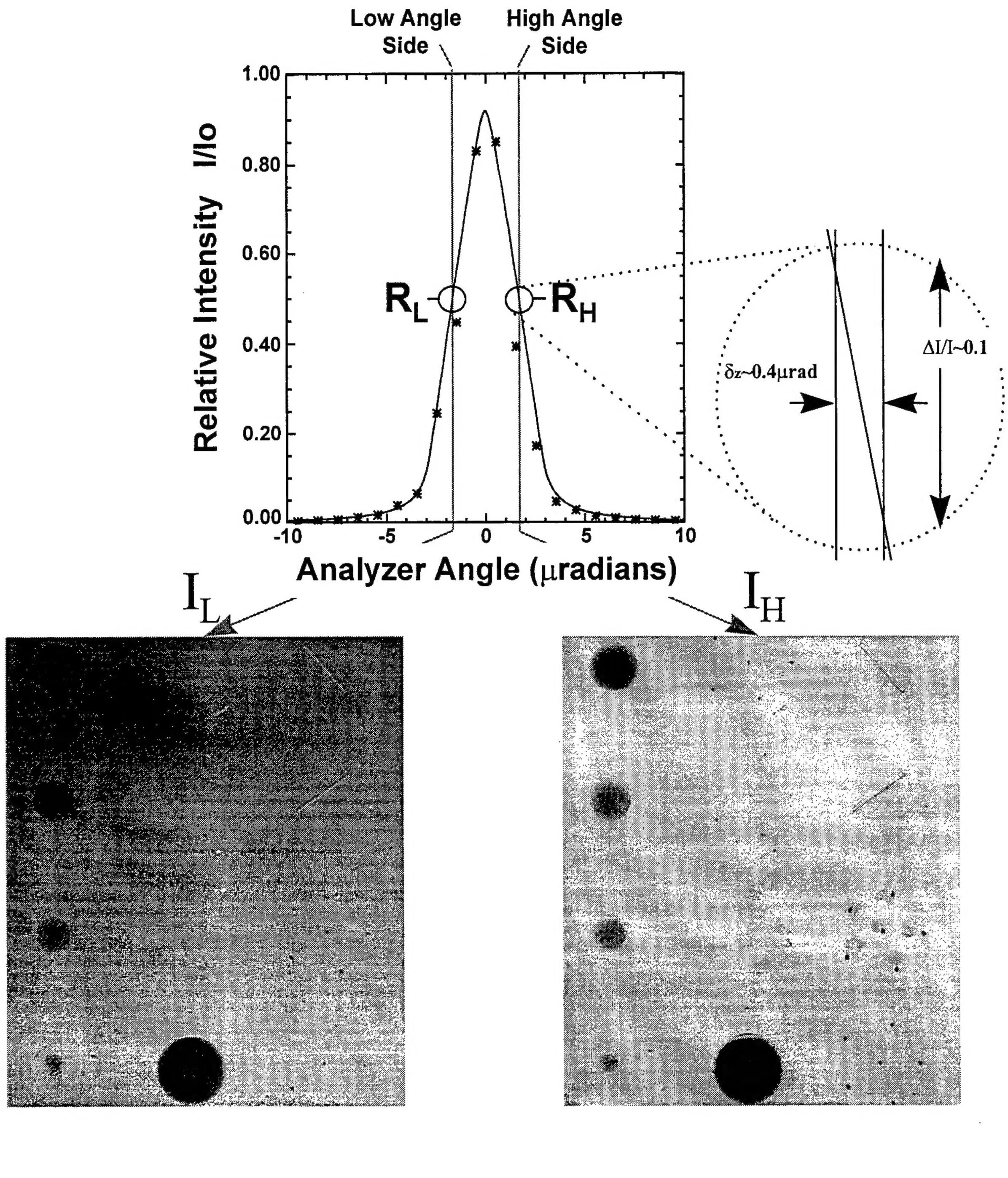

Low Angle Side
High Angle Side
1.00
0.80
0.60
0.40
0.20
0.00
Relative Intensity I/Io
R_L
R_H
δz~0.4μrad
ΔI/I~0.1
-10
-5
0
5
10
Analyzer Angle (μradians)
I_L
I_H

Figure 1.

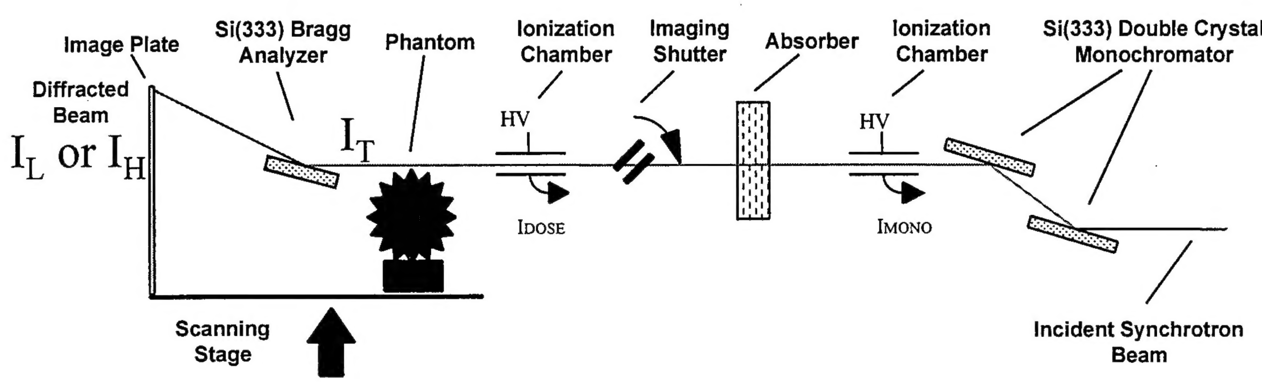

Image Plate
Si(333) Bragg Analyzer
Phantom
Ionization Chamber
Imaging Shutter
Absorber
Ionization Chamber
Si(333) Double Crystal Monochromator
Diffracted Beam
I_L or I_H
I_T
HV
HV
IDOSE
IMONO
Scanning Stage
Incident Synchrotron Beam

Figure 2.

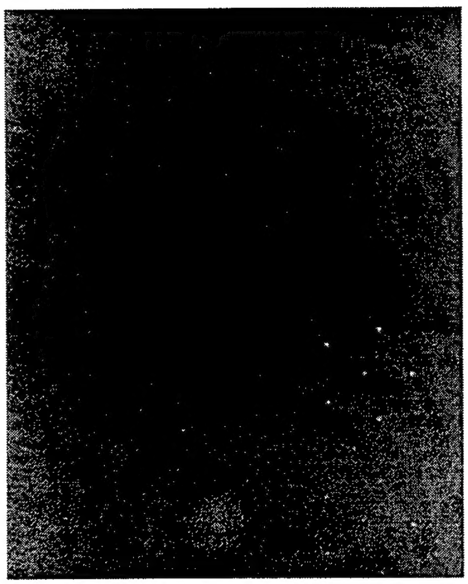

a. **Conventional X-Ray Tube Image**

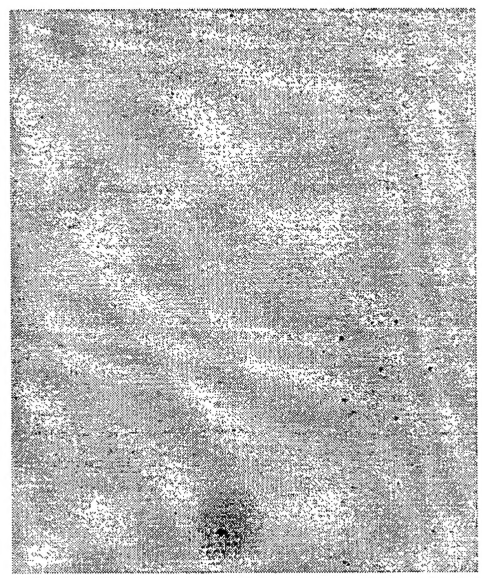

b. **Synchrotron Image - no analyzer**

Figure 3.

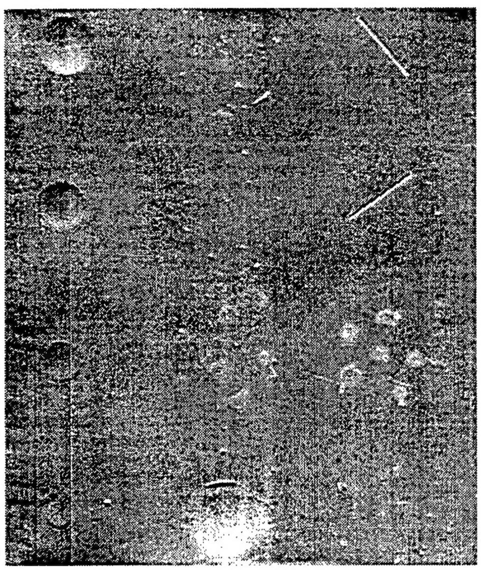

a. **Refraction Angle Image**

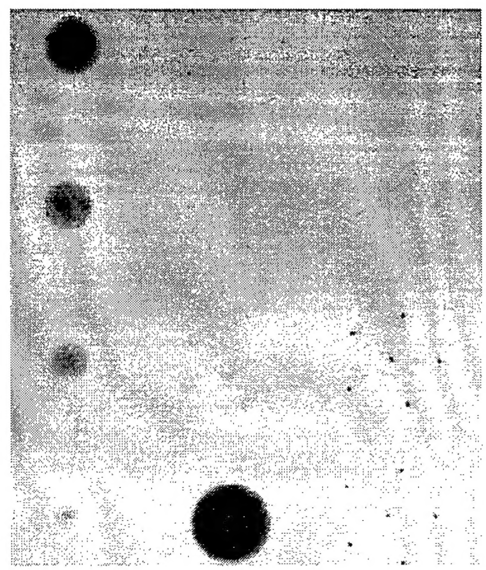

b. **Absorption Image**

Figure 4.